Title

Paleointensity From Subaerial Basaltic Glasses From the Second Hawaii Scientific Drilling Project (HSDP2) Core and Implications for Possible Bias in Data From Lava Flow Interiors

Journal

Journal of Geophysical Research: Solid Earth, 122(11)

ISSN

2169-9313

Authors

Cai, S
Tauxe, L
Cromwell, G

Publication Date

2017-11-01

DOI

10.1002/2017jb014683

Peer reviewed

AGU PUBLICATIONS

JGR

Journal of Geophysical Research: Solid Earth

RESEARCH ARTICLE
10.1002/2017JB014683

Key Points:
- 21 robust paleointensities from subaerial basaltic glasses from the second Hawaii Scientific Drilling Project (HSDP2) core
- Systematical discrepancy between the new paleointensities from glassy margins and those from the interiors of the same lava flows
- Although lower than published data from the same flows, our paleointensities are not as low as expected from a geocentric axial dipole

Supporting Information:
- Supporting Information S1

Correspondence to:
L. Tauxe,
ltauxe@ucsd.edu

Citation:
Cai, S., Tauxe, L., & Cromwell, G. (2017). Paleointensity from subaerial basaltic glasses from the Second Hawaii Scientific Drilling Project (HSDP2) core and implications for possible bias in data from lava flow interiors. *Journal of Geophysical Research: Solid Earth*, *122*. https://doi.org/10.1002/2017JB014683

Received 10 JUL 2017
Accepted 22 OCT 2017
Accepted article online 25 OCT 2017

Paleointensity From Subaerial Basaltic Glasses From the Second Hawaii Scientific Drilling Project (HSDP2) Core and Implications for Possible Bias in Data From Lava Flow Interiors

S. Cai[1,2], L. Tauxe[1], and G. Cromwell[1]

[1]Scripps Institution of Oceanography, University of California, La Jolla, CA, USA, [2]State Key Laboratory of Lithospheric Evolution, Institute of Geology and Geophysics, Chinese Academy of Sciences, Beijing, China

Abstract In this study, we collected samples from subaerial basaltic glassy margins from the second Hawaii Scientific Drilling Project (HSDP2) core. We employed the rigorous "IZZI" method during the paleointensity experiment combined with the stringent "CCRIT" criteria for data selection to obtain 21 robust paleointensity estimates recorded by glassy margins from 20 lava flows. We compared our new results to published paleointensities from the interiors of the lava flows from HSDP2 and found that our data are systematically lower than those from the interiors of the same lava flows. The reasons for the discrepancy in intensity are still unclear, but one possibility that could not be absolutely excluded is the effect of cooling rate on the more slowly cooled lava flow interiors. Although our new data from the glassy margins are lower than those from the lava flow interiors, they are still overall higher than the expected field of the study site calculated from a geocentric axial dipole model with an ancient average field of 42 ZAm^2, either because of a long-term local anomaly of the field in Hawaii or an insufficient age distribution of our new data (e.g., missing the time period with low field intensities).

1. Introduction

The geomagnetic field is thought to span at least ~3.5 Ga (Biggin et al., 2011; Tarduno et al., 2007; Usui et al., 2009) and varies on time scales from tens to millions of years. In order to understand the evolution of the (absolute) intensity of the field during the geological time before the Holocene, the paleomagnetic community relies primarily on experimental results from volcanic materials. Many published paleointensity data are stored in the online MagIC database (http://earthref.org/MagIC) and can be used to decipher the history of the geomagnetic field. However, these published data are very complicated with uneven and hard to assess accuracy because of the plethora of experimental techniques and data selection criteria used.

An example of the consequences of the difficulty to filter accurate from inaccurate data is the issue of the geocentric axial dipole (GAD) model of the field. If the time-averaged geomagnetic field is well approximated by a GAD model (as strongly suggested by directional data, for example, Opdyke & Henry, 1969), then the paleointensity of the field should follow the relation of $(1 + 3\cos^2\theta_m)^{1/2}$ (where θ_m is colatitude), which is twice as strong at the poles than at the equator. However, the time-averaged field calculated from published paleointensity data from either the past 0.78 Ma (Figure 1) or 5 Ma (Cromwell, Tauxe, & Halldórsson, 2015; Lawrence et al., 2009) is poorly fit by a GAD model, with the paleointensities at midlatitudes similar to those at the poles.

The cause of the discrepancy between the observations of field intensities and the theoretical predictions made from a GAD model remains unclear. Several possibilities are as follows: (1) the average dipole moment fluctuates through time with several authors suggesting that the more recent average moment was higher than the preceding times (e.g., Selkin & Tauxe, 2000; Ziegler et al., 2011) and mixing data from different field states would result in apparent non-GAD behavior; (2) the high latitude results could be suppressed by the so-called tangent cylinder related to the Earth's inner core (as discussed in Lawrence et al., 2009); or (3) one or more data sets could suffer from a potential bias in field strength estimates derived from nonideal behavior (e.g., Wang, Kent, & Rochette, 2015). Support for the latter hypothesis can be found in, for example, Cromwell et al. (2013), who found that intensities derived from nonlinear Arai plots, which show the

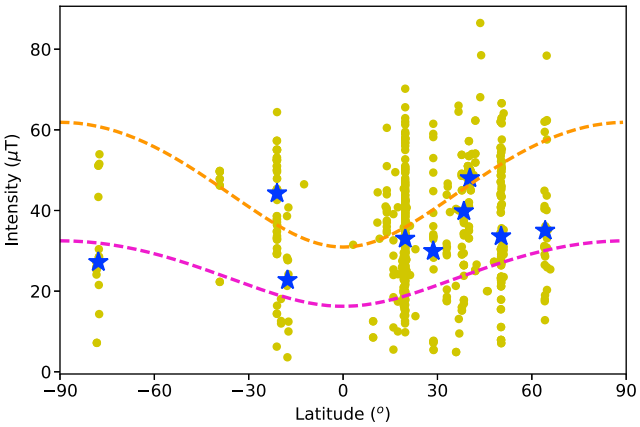

Figure 1. Thellier-type paleointensity data downloaded from the MagIC database, selected with $\sigma < 6$ μT or $\sigma < 15\%$ and 0.01 Ma < age < 0.78 Ma. The orange/magenta line is the field intensity expected from a geocentric axial dipole field with a moment of 80 ZAm^2 (present field)/42 ZAm^2 (ancient field). The blue stars are median values of 10° latitude bins (only bins with more than 10 data points are included).

relationship between remaining natural remanence and laboratory induced remanence (Nagata, Arai, & Momose, 1963), were lower than those derived from linear plots from the same lava flows.

Approximately 60% of the data from low latitudes (30°N to 30°S) for the last 0.78 Ma come from Hawaii, and most of those come from the Hawaii Scientific Drilling Project cores. Laj et al. (2011) summarized much of this work and published paleointensity data from subaerially erupted lava flows of the second Hawaii Scientific Drilling Project (HSDP2) core. These flows are thought to span the last 300 kyr (Sharp & Renne, 2005). In this study, we collected samples from the same section of the HSDP2 drill cores as Laj et al. (2011), but we sampled only the basaltic glassy margins of the lava flows. We carry out rigorous paleointensity experiments on these samples and compare the results to those in Laj et al. (2011) on a lava flow by lava flow basis in order to investigate the similarities or differences between the two approaches. We also expect to obtain implications for the GAD issue of the paleomagnetic field from our new robust results from the low to midlatitude of Hawaii.

2. Sample Collection

The second Hawaii Scientific Drilling Project drilled a sequence of lava flows near Hilo on the Island of Hawaii (19°42′46″N, 155°3′15″W). More than 3,098 m of core were recovered, the upper 1,090 m of which is composed of subaerially erupted lavas; lava flows deeper than 1,090 m below land surface (bls) were erupted in a submarine environment (Garcia et al., 2007) whose paleointensity was previously studied by Tauxe and Love (2003). The subaerial section is further subdivided between lava flows originating from Mauna Kea volcano (~255 to 1,090 m bls) and Mauna Loa volcano (10 to ~255 m bls). Cores from HSDP2 are stored at the American Natural History Museum storage facility in New York City, New York, USA. Following the successful approach of Cromwell et al. (2015), we sampled rapidly cooled flow tops from each subaerial lava flow, preferentially selecting glassy volcanic material whenever possible. We also sampled lava flow bottoms where glassy material was present, or where the underlying flow had a baked contact (indicating that the underlying flow underwent substantial reheating and remagnetization). All (unoriented) subsamples were carefully removed with a hammer and chisel. Samples collected from flow tops are indicated with an "a" identifier, and samples from flow bottoms are marked with "b". Each flow margin is treated as a "site" using the definition that sites are collections of samples for which the parameter of interest is expected to be the same.

3. Paleointensity Methods

A total of 78 glassy margins from 73 lava flows were processed for the paleointensity experiment. Basaltic glassy samples were crushed into small fragments, and the cleanest, most glassy pieces were selected. Each piece was prepared as a specimen by fixing it in a glass vial (12 mm in diameter) with glass microfiber filters and potassium silicate glue. Three to 18 specimens were prepared from each margin, and 546 specimens were measured in total. We adopted the "IZZI" protocol (Tauxe & Staudigel, 2004; Yu, Tauxe, & Genevey, 2004) for the paleointensity experiment. This experimental protocol is as follows: specimens are heated to a certain temperature and cooled down to room temperature in zero laboratory field (zero-field step), and then reheated to the same temperature but cooled down in an applied laboratory field (in-field step). We switch the sequence of zero-field and in-field steps every temperature step until specimens are totally demagnetized. Partial thermal remanent magnetization (pTRM) checks for alteration were inserted every other temperature step (Coe, Grommé, & Mankinen, 1978). Specimens were heated in the laboratory-built paleointensity oven in the magnetically shielded room at the paleomagnetism laboratory of the Scripps Institution of Oceanography (SIO), University of California, San Diego, USA. The ovens are fixed with a fan for rapid cooling; the cooling time in the ovens from ~600°C to room temperature is about 30 min. The residual field of the oven was monitored before zero-field steps, which was always less than 10 nT. The temperature intervals during the paleointensity experiment vary from 100°C to 10°C until specimens were totally demagnetized. A laboratory field of either 20 μT or 50 μT was applied along $-Z$ axis of the

Table 1
Statistical Threshold Values of CCRIT

β	DANG	MAD	FRAC	SCAT	$\lvert\vec{k}\rvert$	Gap Max	N_{min}	σ/% or σ
≤0.1	≤10.0°	≤5.0°	≥0.78	Pass	≤0.164	≤0.6	3	≤10% or 4 μT

Note. Please find the description of each parameter in the text.

specimens with a precision of 0.1 μT for the in-field step and was monitored continuously during the experiment. Specimens were measured on a 2G cryogenic magnetometer after each heating step. The rigorous techniques employed in this study assist in excluding potential biases during the paleointensity experiments and promote acquisition of high-quality results. Cromwell et al. (2015) used this protocol to reproduce the historical field values from Hawaii with high precision and accuracy.

4. Results

We used the "Thellier Auto Interpreter" function, which is included in the Thellier GUI software (Shaar & Tauxe, 2013) as part of the PmagPy software package (Tauxe et al., 2016), to analyze our data. We employed the stringent selection criteria put forward by Cromwell et al. (2015) and named "CCRIT" by Tauxe et al. (2016), for the purpose of achieving robust paleointensities. The selection criteria are listed in Table 1. Detailed descriptions of these criteria can be found in Shaar and Tauxe (2013) and Paterson et al. (2014, and references therein), but we briefly define them here. β is the standard deviation of the slope of selected data points normalized by the absolute value of the slope. DANG is the deviation angle between the best fit line and the line determined by the center of mass of the data points and the origin. MAD is the maximum angular deviation representing the scatter of selected natural remanent magnetization (NRM) about the (unanchored) best fit line. FRAC is the fraction of remanence calculated by the ratio of the vector difference sum (VDS) of the selected NRM segment to the VDS of the entire NRM. SCAT is a Boolean dependent on β and defines the allowed degree of scatter of the selected data points (including pTRM checks). $\lvert\vec{k}\rvert$ is the absolute value of curvature of the data points used for determining the best fit line. Larger $\lvert\vec{k}\rvert$ values usually indicate that the specimen is more prone to be affected by multidomain (MD) particles, thermal alteration, or multiple components. Gap Max is the maximum length of the vector differences between adjacent chosen temperature steps normalized by the VDS of the chosen NRM segment. N_{min} is the minimum number of accepted specimens to calculate the site-mean intensity. σ is the one-sigma standard deviation of site-mean intensity. N_{min} and σ are statistics for site means, while the others are all for specimens.

In total, 100 out of 546 specimens from 21 glassy margins (sites) of 20 lava flows passed the "CCRIT" selection criteria. At most one glassy margin passed the selection criteria, except for lava flow 2, where both top (h2a) and bottom (h2b) glassy margins passed our criteria.

Representative Arai plots of specimens passing and failing the selection criteria are shown in Figure 2. Successful specimens generally show common characteristics, with straight lines on the Arai plots and a single directional component going to the origin on Zijderveld orthogonal projections (Zijderveld, 1967) (Figures 2a and 2b). However, specimens that fail the criteria have various behaviors, such as multiple components (Figures 2c and 2f), or curved and/or zigzagged Arai plots (Figures 2d and 2e). The orthogonal projection plots of Figures 2c and 2f both show multiple components; the Arai plot of the former is nearly linear, indicating the two components recorded similar paleointensity values, while the Arai plot of the latter shows disparate slopes, with multiple possible intensity interpretations. Figures 2d and 2e both show "zigzag" behavior in the Arai plots, which is usually explained as the influence of pTRM tails (Yu et al., 2004), often ascribed to more complexly magnetized remanent states such as vortex state (VS) or multidomain (MD) magnetic grain sizes. But Figure 2e is more curved than Figure 2d, which is probably because the specimen in Figure 2e has a larger content of larger particles. All four rejected specimens mentioned above failed at least one of the statistics in "CCRIT" criteria. All the accepted sample (site) results are listed in Table 2, while those on specimen level are listed in Table S1 in the supporting information.

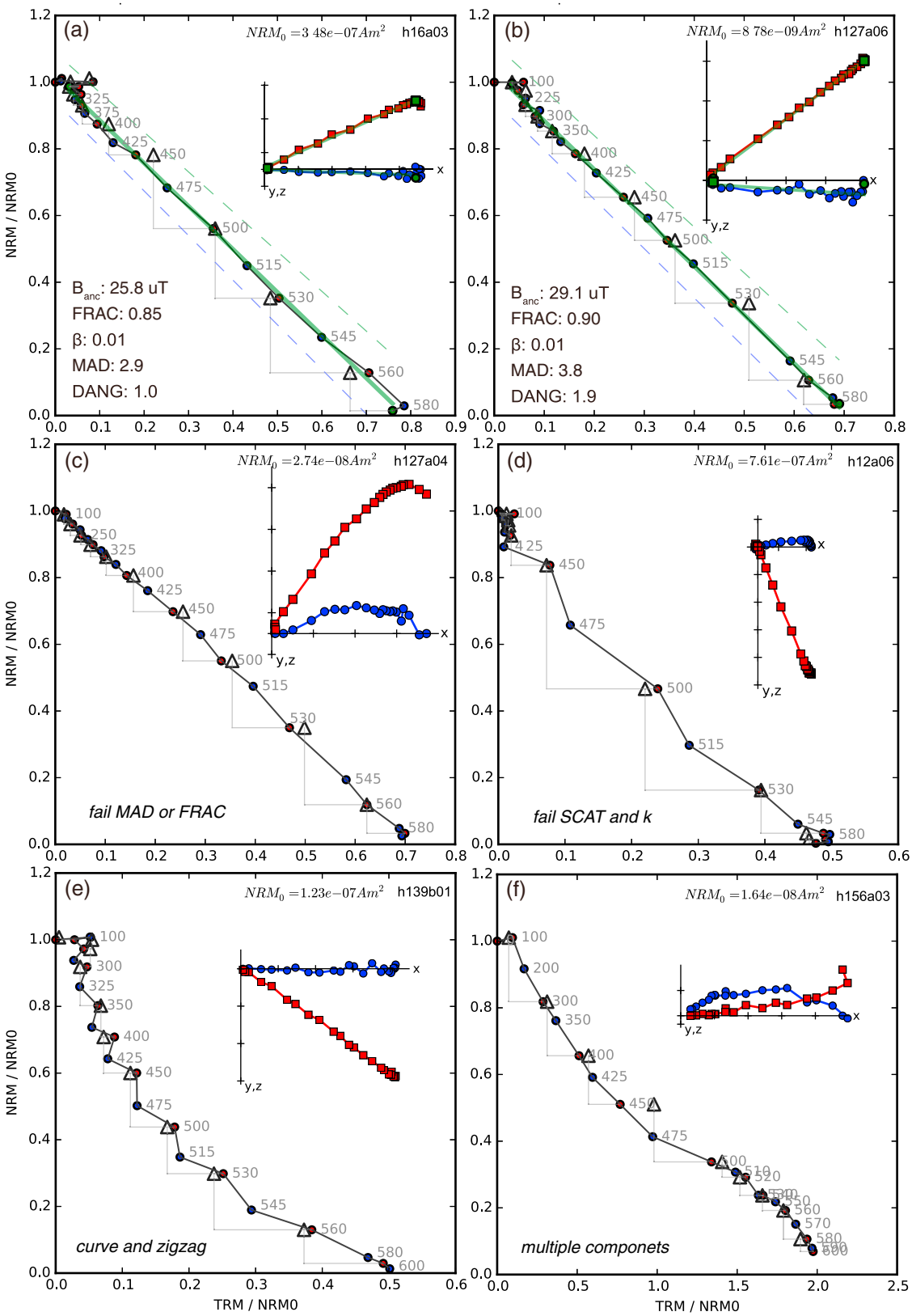

Figure 2. Arai plots of representative (a and b) accepted and (c–f) rejected specimens. The inserts are the associated orthogonal projections. The numbers on the Arai plots are temperature steps in centigrade (°C). The plots were made with the Thellier GUI (Shaar & Tauxe, 2013). For detailed description of these plots, please see the reference.

Table 2
Accepted Results at the Site Level

Sites	Age/ka	N_a	B/μT	σ_B/μT	σ_B/%	VADM/ZAm^2	σ_{VADM}/ZAm^2
h2a	8.5	4	59.10	2.13	3.61	131.86	4.75
h2b	8.5	3	34.32	2.02	5.87	76.57	4.51
h6a	30	6	30.48	1.30	4.27	68.01	2.90
h7a	35.4	4	38.32	2.76	7.20	85.50	6.16
h8a	39.4	7	31.01	0.05	0.15	69.19	0.11
h16a	77.4	9	26.08	1.30	4.98	58.30	2.90
h20a	87.5	4	41.23	1.98	4.80	91.99	4.42
h24a	103.47	3	35.41	2.41	6.80	79.00	5.38
h26b	111.59	3	26.65	0.28	1.06	59.46	0.62
h88a	345.3	6	39.02	2.01	5.15	87.06	4.48
h89a	345.99	4	31.45	2.09	6.65	70.17	4.66
h98a	354.25	5	39.30	0.56	1.42	87.68	1.25
h110b	361.53	3	45.72	0.05	0.10	102.01	0.11
h119a	367.39	6	44.31	2.46	5.56	98.86	5.49
h127a	373.73	5	29.10	0.65	2.23	64.93	1.45
h136b	379.62	5	21.39	3.17	14.82	47.72	7.07
h154b	395.37	6	22.53	0.70	3.10	50.27	1.56
h157b	399.65	6	34.73	3.89	11.2	77.49	8.68
h158a	400.26	4	30.65	1.55	5.05	68.30	3.46
h162a	402.79	3	33.99	2.08	6.13	75.84	4.64
h164a	403.1	4	29.72	1.65	5.55	66.31	3.68

Note. N_a: number of accepted specimens; B: paleointensity; σ_B: one-sigma standard deviation of B; σ_{VADM}: one-sigma standard deviation of VADM.

5. Discussion

In this section, we will compare our new paleointensity results from basaltic glassy margins with those from the lava flow interiors published by Laj et al. (2011). We will also briefly discuss the implications of our new data in relation to the poor performance of the GAD model for paleointensity of the geomagnetic field. For the purposes of discussion, we refer to our new results as "SIO_CCRIT" and those reported by Laj et al. (2011) as "Laj11" hereafter.

We plot paleointensities of SIO_CCRIT and Laj11 versus flow numbers in the HSDP2 drill core (Figure 3) and note that most of our new intensities appear lower than those from Laj et al. (2011) from the same flows. To investigate this further, we compare the results of SIO_CCRIT to those of Laj11 lava flow by lava flow in Figure 4a. Again, it appears that the intensities of SIO_CCRIT are overall lower than those of Laj11. These same data are plotted as cumulative distribution functions (CDFs) in Figure 4b, and the SIO data (red) appear to be consistently lower than the Laj11 data (black), a contention supported by a Kolmorgorov-Smirnov (K-S) test whose D statistic of 0.563 is well above the 95% level of confidence critical value of 0.481.

In addition to the K-S test, we conducted a Welch's t test (Welch, 1947) on the site means of the two data sets to provide statistical evidence that our new data set is different from that of Laj11. The Welch's t test statistics (t-statistic and p-value) are listed on Figure 4b. In this test, if the p-value is less than 5%, we can reject the null hypothesis that the two data sets have identical average values at the 95% confidence level. The p-value of the two data sets is ~4%, strongly suggesting that the two tested groups do not share the same mean.

In order to include the flow level uncertainty in the intensity data, we employ a Monte Carlo method to explore the range of likely values for paleointensity data from each site. We first assume that the specimen intensities at the flow level are normally distributed (which is likely to be true), and then randomly select the same number of intensities from a normal distribution with the flow mean intensity and standard deviation. We then calculate a new pair of means for each flow and the p-value for each simulated pair of data sets. This procedure is repeated 10,000 times to estimate the 95% confidence bounds (shown as dashed lines in Figure 4b). The histogram of these p-values is inserted in Figure 4b and shows that ~93% of the p-values are less than 10%. This supports the suggestion that our new data are likely distinguishable from Laj11 even including the paleointensity uncertainties (at the 93% level of certainty).

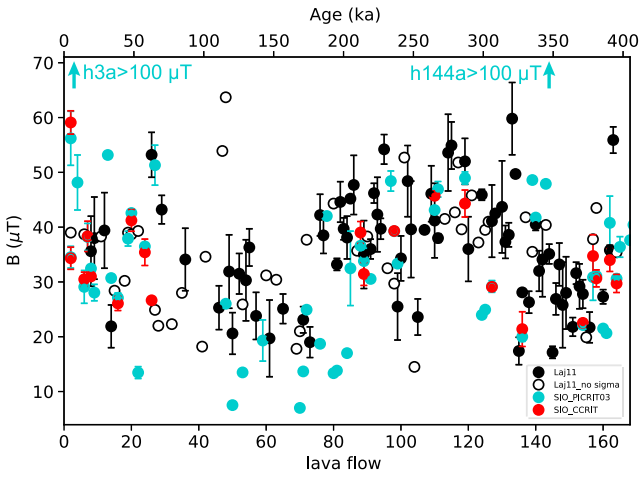

Figure 3. Paleointensities from Laj11 (black solid/open dots), SIO_CCRIT (red dots), and SIO_PICRIT03 (cyan dots) versus HSDP2 lava flows and ages. The open dots represent Laj11 data without paleointensity sigma uncertainty values. The cyan arrows show two SIO_PICRIT03 results with intensities greater than 100 μT.

It is necessary to mention that there is a possibility that those samples collected from the top glassy margins of lava flows (marked as "a") were baked and reheated by subsequent overlying lava flows. Although only samples from two lava flows show evidence of reheating from the overlying flows, the absence of a baked contact cannot guarantee that no reheating event has occurred. In such a case, there might be a difference when comparing results from the margins and interiors of the same lava flow, where the sample from the glassy margin may actually record the paleointensty value of the overlying flow.

A rather clear example of reheating is from Flow 2, where the sample from the top of the flow (h2a) recorded a higher intensity (59.1 μT) than the sample from the bottom of the flow (h2b, 34.3 μT). A likely explanation is that h2a was reheated by the overlying Flow 1. Unfortunately, we cannot confirm this hypothesis by comparing intensities recorded by h2a and Flow 1 because we did not find

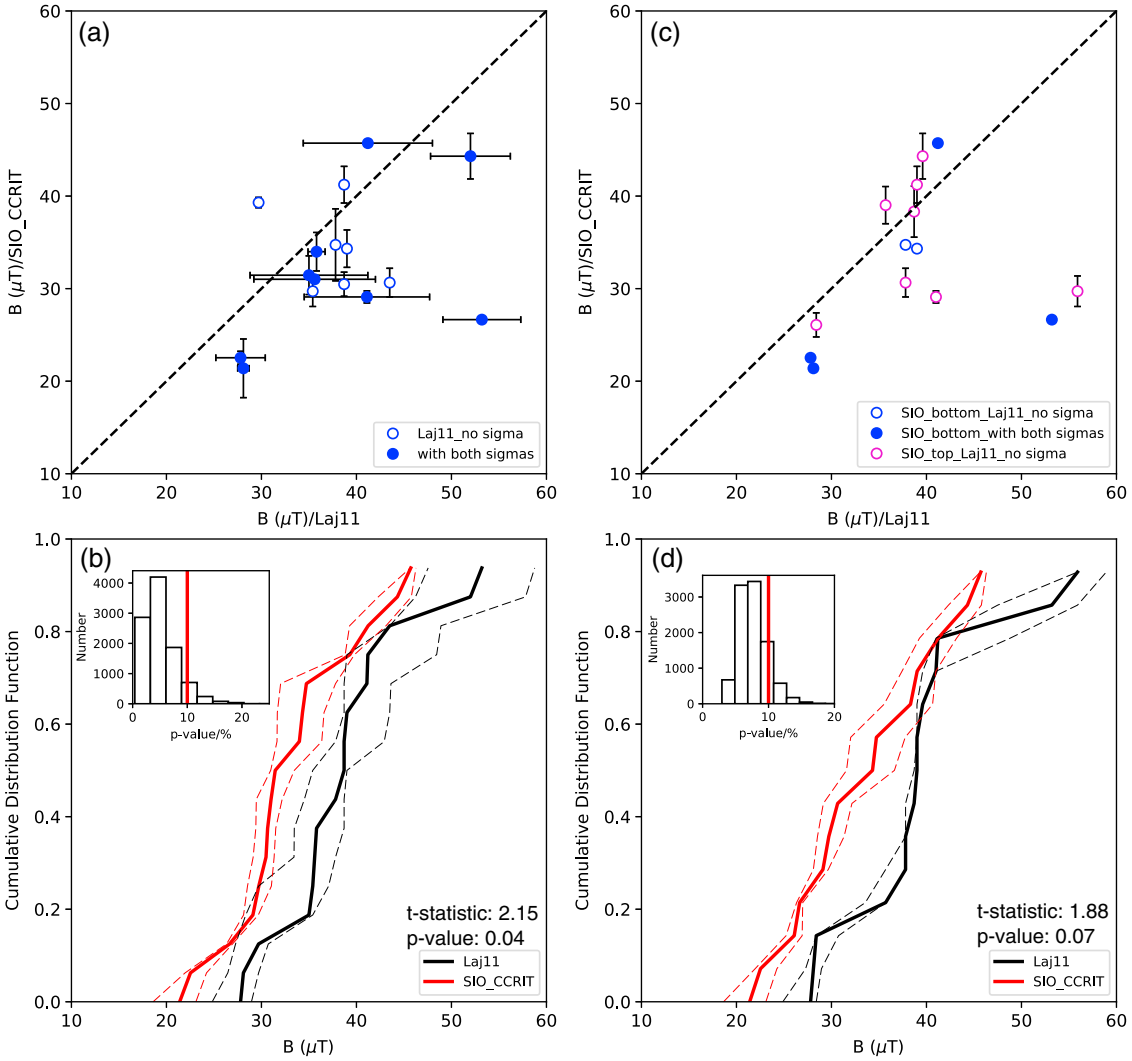

Figure 4. (a) Comparison of paleointensities from SIO_CCRIT to those from the same lava flows in Laj11. (b) Cumulative distribution function (solid lines) and the related 95% confidence boundary (dashed lines) of the two data sets in Figure 4a. (c) The same plot as Figure 4a, but with data from bottom of lava flow in SIO_CCRIT compared to the same lava flows in Laj11 (blue dots) while data from top of lava flows in SIO_CCRIT compared to the overlying lava flows in Laj11 (magenta dots). (d) Cumulative distribution function (solid lines) and the related 95% confidence boundary (dashed lines) of the two data sets in Figure 4d. The open dots in Figures 4a and 4c represent data without uncertainty estimates in Laj11. The dashed lines in Figures 4a and 4c are paleointensity isolines. The Welch's *t* test statistics of the site mean data sets are listed in plots Figures 4b and 4d. The inserts in Figures 4b and 4d are the *p*-value histograms of the new data sets generated with Monte Carlo method, while the red vertical lines therein represent the 10% value.

sufficiently glassy material from Flow 1. Laj et al. (2011) also failed to acquire reliable results from samples collected in the interior of Flow 1. However, the age of Flow 1 reported in Laj et al. (2011) is ~1.3 ka, while that of Flow 2 is ~8 ka. The field intensity between 1.0 and 1.5 ka at the location of HSDP2 predicted by the CALS10k.2 (Constable, Korte, & Panovska, 2016) is ~40 to ~47 μT, while the field intensity estimated at the age of Flow 2 is ~37 μT. This indicates that the field intensity recorded by Flow 1 is probably much higher than that of Flow 2, which supports our speculation that h2a was reheated by the overlying Flow 1. Therefore, we used h2b instead of h2a in Figures 4a and 4b.

In order to check whether the reheating issue affects our other results, we separated our data into two groups: data from the bottom glassy margins and those from the tops. We compared the bottom group to the same lava flows in Laj11 and the top group to the overlying lava flow results from Laj11 where possible (Figure 4c). We also plot the CDF and related 95% confidence boundaries of the two data sets in Figure 4c (Figure 4d). The *p*-value of two sets of site means is only ~7%, which can reject the hypothesis that the two data sets have identical means at the 93% level of certainty. In the histogram of *p*-values (insert in

Table 3
Statistical Threshold Values of "PICRIT_03"

$\beta \leq 0.1$, where β is the same as in CCRIT.
$MAD_{anc} \leq 7.0°$, where MAD_{anc} is the anchored maximum angular deviation.
$f \geq 0.35$, where f is the fraction of selected NRM.
DRAT ≤ 7.0, where DRAT is the maximum difference between pTRM and the pTRM check at a given temperature step normalized by the length of the best fit line.
CDRAT ≤ 10, where CDRAT is the cumulative DRATs.
int_n ≥ 4, where int_n is the number of temperature points used for calculating intensity.
int_ptrm_n ≥ 3, where int_ptrm_n is the number of pTRM checks in the selected segment.
$q \geq 2$, where q is the quality factor determined by fg/β, g is the gap factor.
$\sigma \leq 25\%$, where σ is the same as in CCRIT.

Note. The detailed description can be found in Kissel and Laj (2004) and references therein.

Figure 4d), about 87% of the *p*-values are less than 10%, where the majority supports the conclusion that the two data sets are distinct. From this analysis, it is clear that all but a few of the results of the SIO_CCRIT data set, regardless of whether sampled from the top or bottom of the lava flow, are lower than those of Laj11. Therefore, any undetected sample reheatings will not affect the overall interpretation that SIO_CCRIT intensity values are generally lower than the Laj11 data. All the above analyses allow us to conclude that our new results of SIO_CCRIT are distinguishable from and systematically lower than those of Laj11.

One difference between our data and Laj11 is the specimen level selection criteria used in the analysis. The paleointensity data published by Laj et al. (2011) were selected using the "PICRIT_03" criteria of Kissel and Laj (2004) (listed in Table 3). The low values (≥0.35) for *f* (the fraction of the remanent component used in the intensity calculation) from the PICRIT_03 criteria may allow an overestimation of intensity when Arai plots show curved or two slope behavior as the authors may choose the slope of the lowest temperature components (to avoid alteration effects) as the lower blocking temperature slope is steeper for concave down Arai plots. The steeper the component in the Arai plot is, the greater the resulting intensity estimate is. This effect could plausibly explain the overall higher estimates of intensities in the Laj11 data set if a substantial number of specimens from that study have concave up Arai plots (as might be expected from samples collected from the coarse grained material from lava flow interiors; Dunlop & Özdemir, 2001).

We do not have access to the original measurement data of the Laj11 study, so the effect cannot be directly investigated. However, we can test the hypothesis that selection criteria lead to different conclusions with higher on average interpretations using our own data. To do this, we reanalyzed our own measurement data using the PICRIT_03 criteria and compared the results with those of Laj11. If the overestimate of Laj11 is caused by selection criteria, then our data, analyzed with the same criteria, should be consistent with those from Laj11 considering that they are from the same set of lava flows.

Our results based on the PICRIT_03 criteria (SIO_PICRIT03) are shown with cyan dots in Figure 3. Because PICRIT_03 is less strict, more specimens were accepted using it and the data are much more scattered than the results using CCRIT, with the means of two sites (h3a and h144a) exceeding 100 μT (noted by cyan arrows in Figure 3). We plot the SIO_PICRIT03 data against those from Laj11 from the same lava flows in Figure 5a and the CDFs of the two data sets in Figure 5b. It is clear that even using the same selection criteria, the Laj11 data set is still generally higher than the SIO_PICRIT_03 data set, which indicates that the selection criteria may not explain the discrepancy between the two data sets.

This conclusion is similar to that of Cromwell et al. (2017), who examined the published paleointensity data in Hawaii during the Holocene and found a similar phenomenon to this paper in that data from basaltic fine grained flow tops analyzed with the "IZZI" method and selected using CCRIT are systematically lower than data from interior lava flows with "Thellier-type" method, most of which were done in the identical fashion as the Laj11, including in the same laboratory. Cromwell et al. (2017) discussed the affect of data selection criteria as one possible explanation for the discrepancy. They reanalyzed their specimens that failed the CCRIT criteria but did not alter during the paleointensity experiment with the PICRIT_03 criteria and selected the steepest slope that passed the criteria. They then compared the results with specimens from the same sample but passing the CCRIT criteria and did not see a systematic bias to higher intensities of results from PICRIT_03 criteria.

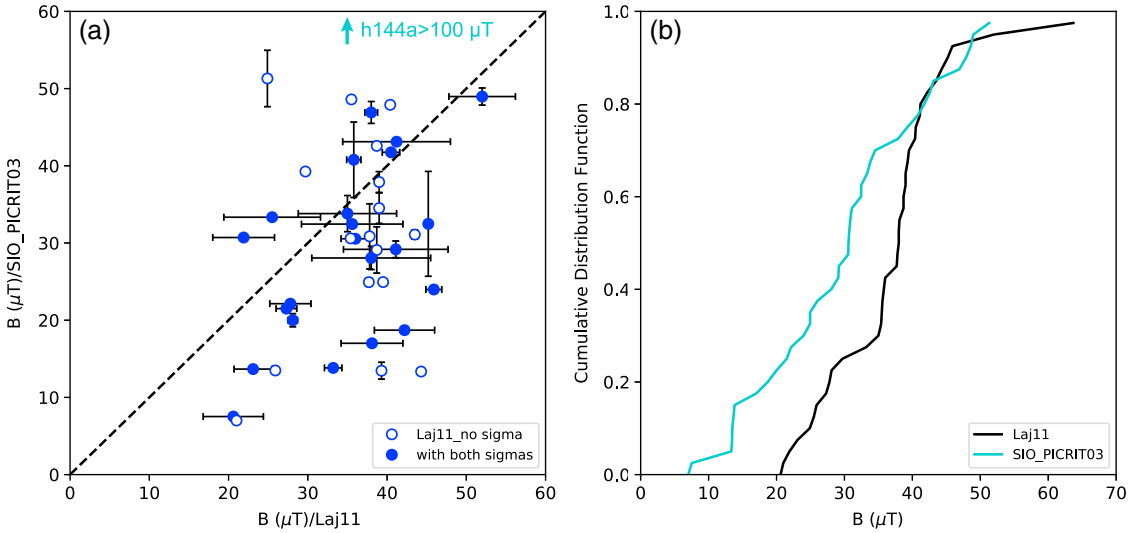

Figure 5. (a) Comparison of paleointensities from SIO_PICRIT03 to those from the same lava flows in Laj11. The open dots represent data without paleointensity uncertainty estimates in Laj11. The cyan arrow shows one SIO_PICRIT03 result with intensity greater than 100 μT. The dashed line is paleointensity isoline. (b) Cumulative distribution function of the two data sets shown in Figure 5a.

Another possibility causing the bias could be the cooling rate effect (e.g., Halgedahl, Day, & Fuller, 1980). Many recent studies focused on the relationship between thermal remanent magnetization (TRM) and cooling rate of materials with various domain states (e.g., Biggin et al., 2013; Ferk et al., 2014; Yu, 2011). A general conclusion from all these studies is that particles of noninteracting single domain (SD) and fine nonuniform remanent states show a stronger cooling rate effect than coarser grained, vortex state (VS) and multidomain (MD) grains. It is believed that most of the igneous rocks used for paleointensity studies are composed of VS and MD particles, and thus, the cooling rate effect on these samples is quite limited and can be neglected (Biggin et al., 2013; Ferk et al., 2014).

In this study, we find that our results from glassy basaltic margins are systematically lower than data of Laj et al. (2011) from lava flow interiors. The median values of SIO_CCRIT and Laj11 in Figure 4a are 31.23 μT and 38.25 μT, respectively, which means that the median value of our data is ~18% lower than that of Laj11. Rapidly cooled glassy basaltic margins like those used in this study usually consist of mixtures of superparamagnetic and/or SD particles (see hysteresis loops and first-order reversal curves in Figure S1 in the supporting information; Harrison & Feinberg, 2008) and are likely to have a cooling rate dependence. However, basaltic glasses have a natural cooling rate similar to the experimental cooling rate used in the SIO laboratory (Bowles et al., 2005) and thus should not require a cooling rate correction. On the other hand, samples in Laj et al. (2011) are from lava flow interiors and must have cooled more slowly than the glassy margins; these results could be overestimated if the sample's magnetizations are dominated by SD or fine VS.

Laj et al. (2011) mentioned that their samples were treated in two kinds of furnaces: one that allows samples to cool naturally overnight while the other is fixed with a fan and can cool the samples in 1 to 2 h. They stated that samples from the same lava flow, but treated in the two different furnaces, yielded consistent results, which indicates that these samples have no significant cooling rate effect on the magnetizations. However, it is worth mentioning that the cooling rate of lava flows could be much more complicated than we know as it relies on the details of the compositions of the materials, and their positions inside the lava flows (i.e., the interior part cools slower than the exterior). Even sister specimens could respond dissimilarly to the cooling rate because of the inhomogeneity of lava flows. We cannot absolutely exclude the possibility of a cooling rate effect causing the bias between our new results and those of Laj et al. (2011); this issue could be resolved through a systematic interlaboratory comparison of results with carefully controlled cooling rates and other laboratory conditions. Such an experiment is beyond the scope of this paper.

The time-averaged field calculated from the published paleointensity data does not follow the expected variation trend from a GAD model during either the past 5 Ma (Cromwell et al., 2015, Lawrence et al., 2009) or the past 0.78 Ma (shown in Figure 1). Either the paleointensities from low latitudes are "too high"

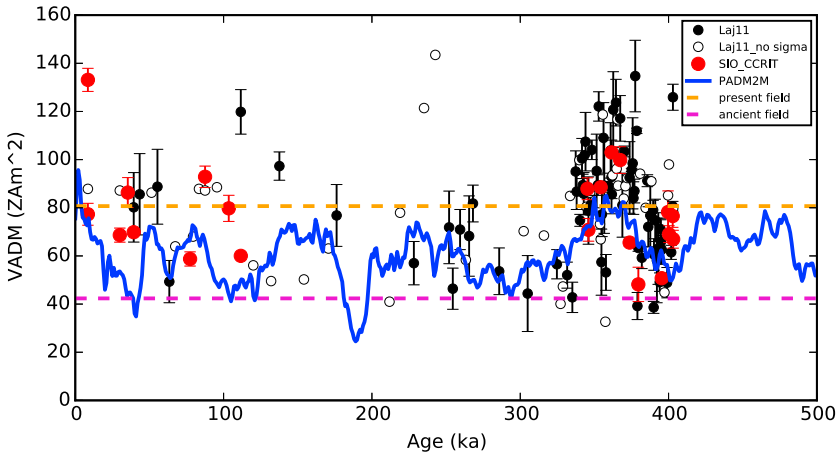

Figure 6. Variations of virtual axial dipole moments (VADMs) from this study (red dots) and Laj11 (black open/solid dots) versus age. We use the same age model as reported by Laj et al. (2011). The black open dots represent data without paleointensity uncertainty estimates in Laj11. The blue line is the PADM2M model of Ziegler et al. (2011). The orange and magenta dashed lines are the present average field of 80 ZAm^2 and an ancient average field of 42 ZAm^2.

or those at the poles are "too low". Wang et al. (2015) reported paleointensities from equatorial Galapagos lava flows spanning the past 5 Ma (exact ages unknown) and concluded that their mean paleointensity (21.6 ± 11.0 μT) is approximately half of that from Antarctica (33.4 ± 13.9 μT) in Lawrence et al. (2009) within uncertainties, supporting the existence of a GAD-like field over the last 5 Ma. It should be mentioned that the mean intensity of 33.4 ± 13.9 μT from Antarctica was recalculated by Wang et al. (2015) from 38 sites, while the original mean intensity reported by Lawrence et al. (2009) is 31.5 ± 2.4 μT calculated from 41 sites, where 2.4 μT is the standard error of the mean paleointensity and the standard deviation should be 15.04 μT. We note that the results of Wang et al. (2015) attempted to correct for the bias introduced by MD grains in their samples. If the results of Wang et al. (2015) are correct, then the mean paleointensities from Hawaii (33.3 ± 13.9 μT, calculated from paleointensity data downloaded from the MagIC database, selected with $\sigma < 6$ μT or $\sigma < 15\%$ and age between 0.01 and 5 Ma) are too high for a GAD model.

As demonstrated by this study, paleointensities derived from the lava flow interiors (as in Laj et al., 2011), which constitute the majority of the published data set from Hawaii, show a generally high bias compared to data from basaltic glasses, but the reason for the bias remains unclear. The average/median value of our new data, excluding those from the Holocene, is 33.22 ± 6.86 μT/31.45 μT, about 7%/13% lower than that of Laj et al. (2011) (35.75 ± 10.22 μT/36.15 μT). If only considering lava flows that were deemed "successful" in both studies, the average/median value of our new data (32.91 ± 6.98 μT/31.23 μT) is ~14%/18% lower than that of Laj et al. (2011) (38.29 ± 7.19 μT/38.25 μT). Interestingly, assuming an ancient average dipole moment of 42 ZAm^2 for the past 160 Ma calculated by Juárez et al. (1998) and for 0–140 Ma recalculated by Tauxe et al. (2013) would predict an average field of 18.81 μT at the location in Hawaii, and our data are still overall higher than that. This is perhaps expected as many studies have suggested that the average field during the last 300 kyr or so was higher than fields in the more distant past (Selkin & Tauxe, 2000; Ziegler et al., 2011). In Figure 6 we compare the HSDP2 data sets (converted to virtual axial dipole moments (VADMs)) with the paleomagnetic axial dipole moment predictions from the PADM2M model of Ziegler et al. (2011). The Laj11 data set is substantially higher than the predicted values, while our new data are overall lower than Laj11 but still higher than the predicted values from Ziegler et al. (2011). We should bear in mind that the PADM2M model derives from sediments and therefore was calibrated by absolute data. Taking the calibration at face value, one possible explanation for the discrepancy between our data and the PADM2M trend is that there is a long-term local anomaly of the field in the vicinity of Hawaii. Alternatively, either the calibration of the PADM2M record requires revision, or it is possible that our new data do not span a sufficient length of time with the fact that none of our collected samples from 100 to 350 ka, a time period when the field intensity may have been lower (Figure 3), passed our strict selection criteria. Given the difficulty in accurate dating of the HSDP2 sequence, it is also possible that our data fail to recover lower and possibly excursional intensities. Unfortunately, the issue cannot be addressed until more paleointensity data with high quality and reliable dating are available in the future.

6. Conclusions

In this study, we collected samples of subaerial glassy basalts from the margins of lava flows from the HSDP2 drill core. After a rigorous paleointensity experiment (IZZI method) and stringent data selection (CCRIT criteria), we obtained robust paleointensities for 21 glassy margins from 20 lava flows. We compared our new data with those from the interiors of many of the same lava flows published by Laj et al. (2011). We found that the average/median value of our new data is some ~14%/18% lower than that of Laj et al. (2011) if only considering lava flows that were deemed "successful" in both studies. The origin of the discrepancy is still unclear, but the possibility of cooling rate effect on slow-cooling lava flows cannot be absolutely excluded. When comparing our new data with the expected field of the HSDP2 location in Hawaii calculated from a GAD model assuming an ancient average field of 42 ZAm^2, or the somewhat higher Brunhes estimate of dipole moment from the PADM2M model of Ziegler et al. (2011), our data are still overall higher than the expected field, either because there is a long-term local anomaly of the field in Hawaii, because of inaccurate calibration of PADM2M, or the possibility that our new results do not cover the time period with low field intensities. More reliable data are required in the future to address this question.

Acknowledgments
We thank Jason Steindorf, Farida Baxamusa, Janine Roza, and Christeanne Santos for their assistance in measuring the samples. This work is funded by NSF grants EAR1547263, EAR1520674, and EAR1345003 to LT. All of the measurement level data and our interpretations will be available in the MagIC database (http://earthref.org/MagIC/11909) upon acceptance of the manuscript. The code used for calculations is available in the repository at http://github.com/PmagPy.

References

Biggin, A. J., Badejo, S., Hodgson, E., Muxworthy, A. R., Shaw, J., & Dekkers, M. J. (2013). The effect of cooling rate on the intensity of thermoremanent magnetization (TRM) acquired by assemblages of pseudo-single domain, multidomain and interacting single-domain grains. *Geophysical Journal International*, *193*(3), 1239–1249. https://doi.org/10.1093/gji/ggt078

Biggin, A. J., de Wit, M. J., Langereis, C. G., Zegers, T. E., Voûte, S., Dekkers, M. J., & Drost, K. (2011). Palaeomagnetism of Archaean rocks of the Onverwacht Group, Barberton Greenstone Belt (southern Africa): Evidence for a stable and potentially reversing geomagnetic field at ca. 3.5 Ga. *Earth and Planetary Science Letters*, *302*(3-4), 314–328. https://doi.org/10.1016/j.epsl.2010.12.024

Bowles, J., Gee, J. S., Kent, D. V., Bergmanis, E., & Sinton, J. (2005). Cooling rate effects on paleointensity estimates in submarine basaltic glass and implications for dating young flows. *Geochemistry, Geophysics, Geosystems*, *6*, Q07002. https://doi.org/10.1029/2004GC000900

Coe, R. S., Grommé, S., & Mankinen, E. A. (1978). Geomagnetic paleointensities from radiocarbon-dated lava flows on Hawaii and the question of the Pacific nondipole low. *Journal of Geophysical Research*, *83*(B4), 1740–1756. https://doi.org/10.1029/JB083iB04p01740

Constable, C., Korte, M., & Panovska, S. (2016). Persistent high paleosecular variation activity in southern hemisphere for at least 10 000 years. *Earth and Planetary Science Letters*, *453*, 78–86. https://doi.org/10.1016/j.epsl.2016.08.015

Cromwell, G., Tauxe, L., & Halldórsson, S. A. (2015). New paleointensity results from rapidly cooled Icelandic lavas: Implications for Arctic geomagnetic field strength. *Journal of Geophysical Research: Solid Earth*, *120*, 2913–2934. https://doi.org/10.1002/2014JB011828

Cromwell, G., Tauxe, L., Staudigel, H., Constable, C. G., Koppers, A. A. P., & Pedersen, R. B. (2013). In search of long-term hemispheric asymmetry in the geomagnetic field: Results from high northern latitudes. *Geochemistry, Geophysics, Geosystems*, *14*, 3234–3249. https://doi.org/10.1002/ggge.20174

Cromwell, G., Tauxe, L., Staudigel, H., & Ron, H. (2015). Paleointensity estimates from historic and modern Hawaiian lava flows using glassy basalt as a primary source material. *Physics of the Earth and Planetary Interiors*, *241*, 44–56. https://doi.org/10.1016/j.pepi.2014.12.007

Cromwell, G., Trusdell, F., Tauxe, L., Staudigel, H., & Ron, H. (2017). Holocene Paleointensity of the Island of Hawai'i From Glassy Volcanics. *Geochemistry, Geophysics, Geosystems*. https://doi.org/10.1002/2017GC006927

Dunlop, D. J., & Özdemir, Ö. (2001). Beyond Néel's theories: Thermal demagnetization of narrow-band partial thermoremanent magnetizations. *Physics of the Earth and Planetary Interiors*, *126*(1-2), 43–57. https://doi.org/10.1016/S0031-9201(01)00243-6

Ferk, A., Leonhardt, R., Hess, K.-U., Koch, S., Egli, R., Krása, D., & Dingwell, D. B. (2014). Influence of cooling rate on thermoremanence of magnetite grains: Identifying the role of different magnetic domain states. *Journal of Geophysical Research: Solid Earth*, *119*, 1599–1606. https://doi.org/10.1002/2013JB010845

Garcia, M. O., Haskins, E. H., Stolper, E. M., & Baker, M. (2007). Stratigraphy of the Hawai'i Scientific Drilling Project core (HSDP2): Anatomy of a Hawaiian shield volcano. *Geochemistry, Geophysics, Geosystems*, *8*, Q02G20. https://doi.org/10.1029/2006GC001379

Halgedahl, S. L., Day, R., & Fuller, M. D. (1980). The effect of cooling rate on the intensity of weak-field TRM in single-domain magnetite. *Journal of Geophysical Research*, *85*(B7), 3690–3698. https://doi.org/10.1029/JB085iB07p03690

Harrison, R. J., & Feinberg, J. M. (2008). FORCinel: An improved algorithm for calculating first-order reversal curve distributions using locally weighted regression smoothing. *Geochemistry, Geophysics, Geosystems*, *9*, Q05016. https://doi.org/10.01029/02008GC001987

Juárez, M. T., Tauxe, L., Gee, J. S., & Pick, T. (1998). The intensity of the Earth's magnetic field over the past 160 million years. *Nature*, *394*(6696), 878–881.

Kissel, C., & Laj, C. (2004). Improvements in procedure and paleointensity selection criteria (PICRIT-03) for Thellier and Thellier determinations: Application to Hawaiian basaltic long cores. *Physics of the Earth and Planetary Interiors*, *147*(2-3), 155–169. https://doi.org/10.1016/j.pepi.2004.06.010

Laj, C., Kissel, C., Davies, C., & Gubbins, D. (2011). Geomagnetic field intensity and inclination records from Hawaii and the Réunion Island: Geomagnetic implications. *Physics of the Earth and Planetary Interiors*, *187*(3-4), 170–187. https://doi.org/10.1016/j.pepi.2011.05.007

Lawrence, K. P., Tauxe, L., Staudigel, H., Constable, C. G., Koppers, A., McIntosh, W., & Johnson, C. L. (2009). Paleomagnetic field properties at high southern latitude. *Geochemistry, Geophysics, Geosystems*, *10*, Q01005. https://doi.org/10.01029/02008GC002072

Nagata, T., Arai, Y., & Momose, K. (1963). Secular variation of the geomagnetic total force during the last 5000 years. *Journal of Geophysical Research*, *68*(18), 5277–5281. https://doi.org/10.1029/JZ068i018p05277

Opdyke, N. D., & Henry, K. W. (1969). A test of the dipole hypothesis. *Earth and Planetary Science Letters*, *6*(2), 139–151. https://doi.org/10.1016/0012-821X(69)90132-0

Paterson, G. A., Tauxe, L., Biggin, A. J., Shaar, R., & Jonestrask, L. C. (2014). On improving the selection of Thellier-type paleointensity data. *Geochemistry, Geophysics, Geosystems*, *15*, 1180–1192. https://doi.org/10.1002/2013GC005135

Selkin, P., & Tauxe, L. (2000). Long term variations in geomagnetic field intensity. *Philosophical Transactions of the Royal Society*, *358*(1768), 1065–1088. https://doi.org/10.1098/rsta.2000.0574

Shaar, R., & Tauxe, L. (2013). Thellier GUI: An integrated tool for analyzing paleointensity data from Thellier-type experiments. *Geochemistry, Geophysics, Geosystems*, *14*, 677–692. https://doi.org/10.1002/ggge.20062

Sharp, W. D., & Renne, P. R. (2005). The 40Ar/39Ar dating of core recovered by the Hawaii Scientific Drilling Project (phase 2), Hilo, Hawaii. *Geochemistry, Geophysics, Geosystems*, *6*, Q04G17. https://doi.org/10.1029/2004GC000846

Tarduno, J. A., Cottrell, R. D., Watkeys, M. K., & Bauch, D. (2007). Geomagnetic field strength 3.2 billion years ago recorded by single silicate crystals. *Nature*, *446*(7136), 657–660. https://doi.org/10.1038/nature05667

Tauxe, L., Gee, J. S., Steiner, M. B., & Staudigel, H. (2013). Paleointensity results from the Jurassic: New constraints from submarine basaltic glasses of ODP Site 801C. *Geochemistry, Geophysics, Geosystems*, *14*, 4718–4733. https://doi.org/10.1002/ggge.20282

Tauxe, L., & Love, J. J. (2003). Paleointensity in Hawaiian Scientific Drilling Project Hole (HSDP2): Results from submarine basaltic glass. *Geochemistry, Geophysics, Geosystems*, *4*(2), 8702. https://doi.org/10.1029/2001gc000276

Tauxe, L., Shaar, R., Jonestrask, L., Swanson-Hysell, N. L., Minnett, R., Koppers, A. A. P., … Fairchild, L. (2016). PmagPy: Software package for paleomagnetic data analysis and a bridge to the Magnetics Information Consortium (MagIC) database. *Geochemistry, Geophysics, Geosystems*, *17*, 2450–2463. https://doi.org/10.1002/2016GC006307

Tauxe, L., & Staudigel, H. (2004). Strength of the geomagnetic field in the Cretaceous Normal Superchron: New data from submarine basaltic glass of the Troodos Ophiolite. *Geochemistry, Geophysics, Geosystems*, *5*, Q02H06. https://doi.org/10.1029/2003gc000635

Usui, Y., Tarduno, J. A., Watkeys, M., Hofmann, A., & Cottrell, R. D. (2009). Evidence for a 3.45-billion-year-old magnetic remanence: Hints of an ancient geodynamo from conglomerates of South Africa. *Geochemistry, Geophysics, Geosystems*, *10*, Q09Z07. https://doi.org/10.1029/2009GC002496

Wang, H., Kent, D. V., & Rochette, P. (2015). Weaker axially dipolar time-averaged paleomagnetic field based on multidomain corrected paleointensities from Galapagos lavas. *Proceedings of the National Academy of Sciences of the United States of America*, *112*(49), 15,036–15,041. https://doi.org/10.1073/pnas.1505450112

Welch, B. L. (1947). The generalization of 'Student's' problem when several different population variances are involved. *Biometrika*, *34*(1/2), 28–35. https://doi.org/10.2307/2332510

Yu, Y. (2011). Importance of cooling rate dependence of thermoremanence in paleointensity determination. *Journal of Geophysical Research*, *116*, B09101. https://doi.org/10.1029/02011JB008388

Yu, Y. J., Tauxe, L., & Genevey, A. (2004). Toward an optimal geomagnetic field intensity determination technique. *Geochemistry, Geophysics, Geosystems*, *5*, Q02H07. https://doi.org/10.1029/2003GC000630

Ziegler, L. B., Constable, C. G., Johnson, C. L., & Tauxe, L. (2011). PADM2M: A penalized maximum likelihood model of the 0-2 Ma palaeomagnetic axial dipole moment. *Geophysical Journal International*, *184*(3), 1069–1089. https://doi.org/10.1111/j.1365-246X.2010.04905.x

Zijderveld, J. D. A. (1967). A.C. Demagnetization of rocks: Analysis of results. In D. Collinson, K. Creer, & S. Runcorn (Eds.), *Methods in paleomagnetism* (pp. 254–286). Amsterdam: Elsevier.